Gas-Surface Energy Exchange in Collisions of Helium Atoms with Aligned Single-Walled Carbon Nanotube Arrays

Ikuya Kinefuchi, Junichiro Shiomi, Shu Takagi, Shigeo Maruyama, and Yoichiro Matsumoto*

Department of Mechanical Engineering, The University of Tokyo, 7-3-1 Hongo, Bunkyo-ku, Tokyo 113-8656, Japan

ABSTRACT

Since gas flows in micro/nano devices are dominated by the interaction of gas molecules and solid surfaces, surface modification technique is one of the critical issues for optimizing the thermal performance of these devices. In this paper, we demonstrate the successful application of vertically aligned single-walled carbon nanotubes (VA-SWNTs) as surface modification material to enhance the energy accommodation of gas molecules on surfaces. The scattering of gas molecules on quartz surfaces covered with VA-SWNTs is investigated by the molecular beam technique. The energy accommodation coefficients of helium, which tend to be small even for rough surfaces because of the large mass mismatch between helium and surface atoms, are close to unity on the modified surfaces. The measurement with the free-standing films further reveals that the high accommodation is attributed to the unique morphology of the films with high porosity, which allows gas molecules to penetrate into the films and realizes a large number of collisions with SWNTs. The result suggests that the surface modification with VA-SWNTs can be utilized for the thermal management in electric devices and micro/nano-electro-mechanical systems.

Keywords: molecular beam, gas-surface interaction, scattering, thermal transport, rarefied gas flow, surface modification

1. INTRODUCTION

While there has been remarkable progress in performance and integration of nano/micro devices over the last decade, the thermal management of the high power density has become one of the most critical issues for practical applications. The recent development of nanotechnology offers tremendous possibilities to synthesize new nanomaterials with thermal transport properties exceeding the conventional materials. For instance, single-walled carbon nanotubes (SWNTs) exhibit anomalously high thermal conductivity along the tube axis comparable or even superior to those of diamond and graphite[1, 2] due to the large mean free path of phonons.[3] In addition, the recent advance in chemical vapor deposition (CVD) technique enables us to fabricate vertically aligned SWNTs (VA-SWNTs),[4-7] which opens up possibilities for directional thermal devices with the anisotropic thermal transport property.[8-11] While aligned SWNTs have been employed as heat conducting fillers in composite materials, their mechanical strength of making them self-standing extends the scope of the thermal application of SWNTs to gas phase, where SWNTs are, for example, used as building material for cooling fins of microelectronic devices.[12-14] Combined with the thermal stability and the extremely high emissivity,[15] such thermal cooling device is expected to cover a wide range of temperature and pressure. Several trials of heat dissipation enhancement with this approach are reviewed in Ref. 16.

The effect of surface structure on the scattering dynamics of gas molecules has been intensively investigated for self-assembled monolayers (SAMs).[17-28] Molecular beam scattering experiments and molecular dynamics (MD) simulations revealed the dominant factors determining the energy exchange efficiency for a variety of gas/SAM surface systems such as the mass of a gas molecule and the terminal group of SAM molecules,[19-22] attractive forces between gas molecules and the SAM terminal groups,[21, 23-25] surface stiffness due to intramonolayer

hydrogen bonding,[21, 23, 26] the chain length of SAM molecules,[26] the deformation of SAM chains,[19, 20, 27, 28] and the penetration of gas molecules into SAM layer.[28] The versatility of functional groups and tail length makes SAMs attractive for surface coatings to control gas-surface interactions. Having better thermal stability than SAMs, VA-SWNT films would be another promising option of surface coating material especially for devices operating over a wide range of temperature.

As in the case of SWNT composite materials,[29] the thermal performance of VA-SWNTs in gaseous environment is determined by the energy accommodation process of gas molecules on SWNT surface rather than by the intrinsic high thermal conductivity of SWNTs since the inter-bundle distance is comparable to the mean free path of gas molecules. MD simulations of gas molecules scattering on an SWNT showed that most of the energy transfer between SWNT and gas molecules takes place in the tube radial direction and that the translational energy distribution of scattered molecules is far from equilibrium at the surface temperature.[30, 31] The nonequilibrium MD simulation of an SWNT surrounded by N_2 and O_2 molecules estimated that the interfacial thermal resistance between SWNT and air is equivalent to the thermal resistance of 250 nm thick layer of air.[13] The thermal conductivity measurement of SWNT aerogels also indicates low energy accommodation of gas molecules with SWNTs.[32] While these studies suggest that SWNT-gas energy accommodation may become a bottleneck for the overall energy transfer, it is not known to this date how well or poor the overall energy transfer would be when an assembly of SWNTs is used as surface modification.

To elucidate the efficiency and mechanism of the energy transfer between a VA-SWNT film and gaseous environment from molecular view point, this paper presents the first experimental study on the scattering process of gas molecules on a surface covered with VA-SWNT arrays by

using the molecular beam technique.[33] Series of experiments were performed with helium molecules, where the large mass-mismatching between the target and gas atoms usually results in poor accommodation[34] even for atomically rough surfaces with gas adsorbates and nanoparticles. Despite this worst case scenario, anomalously effective energy transfer was identified between helium molecules and the VA-SWNTs. The result suggests that the surface modification with VA-SWNTs can be utilized for the thermal management in electric devices and micro-electro-mechanical systems.

2. EXPERIMENTAL SECTION

VA-SWNT films were grown on quartz substrates by the alcohol catalytic CVD process.[4] The catalyst was supported on the substrate using the dip-coating method with a Co-Mo acetate solution (metal content 0.01 wt% each, dissolved in ethanol). The catalyst was oxidized by heating the dip-coated substrate in air at 400 °C, and then reduced in a flowing Ar/H_2 mixture (3% H_2, 300 sccm flow rate, 40 kPa) during heating of the growth chamber. When the temperature in the growth chamber reached 800 °C, the Ar/H_2 flow was stopped and SWNTs were synthesized by supplying ethanol vapor at 1.3 kPa (10 Torr) until the VA-SWNT array had reached the target thickness. Optical absorption and Raman spectra showed that SWNTs in the films have an average diameter of about 2 nm. SWNTs in the films form bundles of typically less than ten SWNTs.[35] Typical images of the films taken by scanning electron microscopy (SEM) are shown in Figure 1. The thinnest sample (0.1 μm) consists of SWNT bundles oriented randomly and does not have well-aligned structure. On the other hand, SWNT bundles align vertically in most part of the thicker samples except for the topmost layer, whose structure is similar to that of the thinnest sample. The porosity of the film was measured based on the film

weights to be about 97%.[36] We also prepared pre-growth quartz substrates, on which Co-Mo catalyst nanoparticles with diameters of 1 – 2 nm are well dispersed without agglomeration.[37]

The scattering experiments were conducted in an ultrahigh vacuum chamber equipped with a supersonic molecular beam source. The schematic illustration of our experimental setup is found in Ref. 38. The molecular beam source consists of three differential pumping chambers. The axial component of a supersonic jet expansion from a 50-μm-diameter orifice at room temperature was extracted through a skimmer (Beam Dynamics, model 1) with a 0.7-mm-diameter opening and subsequently modulated by a chopper. Before entering the main chamber, the beam was further collimated by a skimmer (1.4 mm or 0.7 mm) and an aperture (2.5 mm or 1 mm). The beam spot diameter at the sample was estimated to be 5 – 2 mm (depending on the skimmer and the aperture used in the beam source). The scattered molecules were detected using a quadrupole mass spectrometer (QMS) mounted on a rotatable stage. A partitioning wall with a slit was placed between the sample and the QMS in order to eliminate the undesirable fluctuation of the background noise from the QMS signal.

The time-of-flight (TOF) distributions of scattered molecules are described by the convolution integral

$$S(t) = \int_{-\infty}^{+\infty} R(t-\tau)\, P(\tau)\, d\tau , \qquad (1)$$

where $R(t)$ is the incident beam flux on the sample, and $P(t)$ the TOF distribution of scattered molecules from the sample to the QMS. It is noted that $R(t)$ is a convolution of the beam modulation and the TOF distribution of the incident molecules and hence is a known distribution. For a pulse-modulated beam, the beam modulation function is well approximated by the delta function and hence $R(t)$ reduces to be

$$R(t) \propto \frac{1}{t^5} \exp\left[-\frac{m}{2k_B T_{in}} \left(\frac{L_{CS}}{t} - u_{in} \right)^2 \right], \quad (2)$$

where m is the mass of a gas molecule, T_{in} and u_{in} the translational temperature and macroscopic velocity of the incident beam, L_{cs} the distance between the chopper and the sample (141 mm), k_B the Boltzmann constant. T_{in} and u_{in} can be determined by the measurement of the incident beam with the sample retracted from the beam path. The typical values in our experimental condition were T_{in} = 10 K and u_{in} = 1.7×10^3 m s^{-1}. The TOF distribution of scattered molecules $P(t)$ can be determined from the detected signal $S(t)$, in principle, by deconvoluting Eq. (1), although noise component in the signal makes it practically difficult to perform direct numerical deconvolution with Fourier transform. For this reason, we assumed that the TOF distribution of scattered molecules follows a linear superposition of the direct inelastic scattering component $P_{dir}(t)$ and the trapping-desorption component $P_{ads}(t)$ with a weighting factor γ ($0 \le \gamma \le 1$):[39]

$$P(t) = \gamma P_{dir}(t) + (1-\gamma) P_{ads}(t). \quad (3)$$

Each scattering component is expressed as

$$P_{dir}(t) = \frac{c_1}{t^4} \exp\left[-\frac{m}{2k_B T_r} \left(\frac{L_{sd}}{t - t_{ion}} - u_r \right)^2 \right], \quad (4)$$

$$P_{ads}(t) = \frac{c_2}{t^4} \exp\left[-\frac{m}{2k_B T_s} \left(\frac{L_{sd}}{t - t_{ion}} \right)^2 \right], \quad (5)$$

where L_{sd} is the distance between the surface and the QMS (186 mm), T_r and u_r the translational temperature and drift velocity of the direct inelastic scattering component, T_s the surface temperature, t_{ion} the ion flight time in the QMS, c_1 and c_2 the normalization constants. Since the QMS is a density-sensitive detector, the function form of Eqs. (4) and (5) is different from the distribution in terms of flux (Eq. (2)) by a factor of t.[33] The ion flight time t_{ion} was estimated

from the TOF measurement with the modulation to the ion optics in the QMS. In our apparatus, the ion flight time for helium was t_{ion} = 14 – 15 μs. By least-squares fitting of Eqs. (1) – (5) to the experimental waveforms, we determined the parameters γ, T_r, u_r and thus recovered the TOF distributions of scattered molecules $P(t)$. The velocity distribution of scattered molecules is obtained using the relationship between the TOF distribution in terms of density $P(t)$ and the velocity distribution function $F(v)$:[33]

$$P(t) \propto \frac{1}{t} F\left(\frac{L_{sd}}{t}\right). \tag{6}$$

Finally, the mean translational energy of scattered molecules is given by

$$E_f = \int_0^\infty \frac{1}{2} m v^2 F(v)\, dv. \tag{7}$$

3. RESULTS AND DISCUSSION

3.1. Scattering of Helium on As-Grown VA-SWNT Films

We investigated the scattering of helium on as-grown VA-SWNT films. The pulse-modulated beam with a mean translational energy of 60 meV was directed to these films. The experiments were performed for several incident angles measured from the normal vector of the surface. In the following, the results for the incident angles θ_i = 40° and 70° are shown as the representative cases of small and large incident angles. The scattering distribution of helium beam with a small incident angle θ_i follows the cosine distribution, which corresponds to completely diffusive scattering, both for the quartz substrate and VA-SWNT films with different thicknesses (Figure 2). Helium molecules scattered on the quartz substrate, however, are poorly accommodated in spite of the diffusive distribution. Their mean translational energy is much

higher than that of fully accommodated molecules and rather close to the incident beam energy. These results suggest that the atomic-scale roughness on the surface makes the scattering direction completely random and thus independent of the incident angle even though gas molecules leave the surface before being thermally equilibrated. In contrast, VA-SWNT films exhibit considerably better accommodation compared to the quartz substrate. In particular, the translational energies of scattered molecules from the 4-μm-thick film are almost equal to the value corresponding to the perfect accommodation, demonstrating a successful enhancement of the energy transfer between gas molecules and the surface by modifying it with the VA-SWNT film. This energy transfer is far more efficient than the energy transfer during a single scattering event of helium on SWNT surface obtained by MD simulations.[31] Therefore, the multiple scattering inside the film should be the key factor for the efficient energy accommodation observed for VA-SWNT films. The dependence of the translational energy on the film thickness indicates that at least part of the incident molecules penetrate into the film and interact not only with the outermost part of the film but also with its internal structure.

For a large incident angle, the scattering distribution from the quartz substrate deviates from the cosine distribution and exhibits a lobe around the specular direction (Figure 3). The translational energy of the scattered molecules from the quartz substrate is close to the incident beam energy, showing that the energy accommodation becomes less efficient as the incident angle increases. On the other hand, the scattering distributions from VA-SWNT films follow the cosine distribution even for large incident angles. Although the amount of the energy transfer during the scattering is smaller, especially around the specular direction, than that in the case of $\theta_i = 40°$, scattered molecules still remain much better accommodated compared to those on the quartz substrate. The incident angle dependence of the energy accommodation on the VA-SWNT

films originates from the fact that the incident molecules with larger incident angle tend to experience shallower penetration depth, and thereby, smaller number of collisions with SWNTs before leaving the film. Although the energy transfer becomes less efficient for large incident angle, this has limited impact on the overall energy transfer. Since the incident flux from equilibrium gases on a solid surface is proportional to $\sin 2\theta_i$, gas molecules with the incident angle around 45° have great impact on the overall energy transfer between gas phase and solid surface while the contribution of those with large incident angle (i.e. close to 90°) is limited. For this reason, the surface modification with VA-SWNT film significantly enhances the overall energy accommodation even with the incident angle dependence.

The energy accommodation coefficients of helium beam with the incident angle of $\theta_i = 40°$ were estimated from the molecular beam experiments (Table 1). The energy accommodation coefficient is defined as

$$\alpha = (\overline{E}_i - \overline{E}_f)/(\overline{E}_i - \overline{E}_s), \quad (8)$$

where $\overline{E}_i$, $\overline{E}_f$, and $\overline{E}_s$ are the mean translational energies of the incident beam, scattered molecules, and the fully accommodated molecules. Here $\overline{E}_s$ is $2k_B T_s$, where T_s is the surface temperature. Since our measurements were limited to the in-plane scattering, where the post-scattering velocities are contained within the plane spanned by the normal vector of the sample surface and the velocity vector of the incident molecules, the following assumptions were adopted to estimate the mean translational energy of molecules scattered over all directions; (1) As is the case for the in-plane scattering, the scattering intensity of the out-of-plane scattering follows the cosine distribution; (2) The translational energy of scattered molecules depends only on the angle between the scattering direction and the normal vector of the surface θ_f and is independent of the off-plane angle. In contrast to the heavier gas molecules, helium molecules

are generally known to be hardly equilibrated with the surface temperature during the scattering process even if the surface is covered with gas adsorbates or nanoparticles, which give rise to significant atomic-scale roughness. This trend can be confirmed from the accommodation coefficients for a wide variety of surfaces,[40, 41] which are included in Table 1. With the Baule formula[34] in mind, we can attribute the low accommodation coefficients to the large mismatch between the mass of a helium molecule and the effective mass of the involved surface atoms. Under such unfavorable condition, the surface modification with VA-SWNT films increases remarkably the accommodation coefficients compared to those for the bare surface. Since the scattering of helium gives the conservative estimate of the degree of the energy accommodation for heavier gas molecules, the result in our experiment suggests that the surface modification with VA-SWNT films would also effectively enhance the energy accommodation of other gas species used in practical applications (e.g. N_2 and O_2). Although the accommodation coefficient slightly decreases for the thinner VA-SWNT film, it is still high enough for practical applications. The efficient energy accommodation even for the 0.1-μm-thick VA-SWNT film, which consists only of the randomly oriented layer, suggests that incident molecules on the thicker films have sufficient number of collisions with SWNTs to be accommodated within the topmost layer of the films.

In the temperature jump regime of rarefied gas flow, the thermal conductance at gas-solid interface is given by[42]

$$G = 4k_{\mathrm{B}} N \alpha/(2-\alpha), \qquad (9)$$

where N is the collision rate of gas molecules per unit area. In rarefied gas flow of helium at 10^5 Pa and 300 K, the thermal conductance at the quartz substrate – gas interface is 3.9×10^4 W m^{-2} K^{-1}. When the substrate is covered with 0.1-μm-thick VA-SWNT film, the interfacial thermal

conductance increases to 2.6×10^5 W m^{-2} K^{-1}. The thermal conductance of VA-SWNT film is estimated to be ~10^8 W m^{-2} K^{-1} taking account of the aligned structure with a porosity of 0.97 and the thermal conductivity of SWNTs.[1, 2] Since the thermal conductance of VA-SWNT film is more than two orders of magnitude larger than the conductance at gas-solid interface, the introduction of an extra layer (VA-SWNT film) does not become a bottleneck of the overall heat transfer. It should be noted that the interfacial thermal conductance between VA-SWNT film and substrate could be another bottleneck of the heat transfer. The evaluation and improvement of this interface is under intensive investigation and readers are referred to Ref. 43 – 45 for details.

3.2. Scattering of Helium on Free-Standing VA-SWNT Films

While the above analysis reveals the significant role of the film topmost layer in energy transfer, the dependence of the translational energy on the film thickness indicates that part of the incident molecules penetrate into the film and interact also with its internal structure. In order to reveal the detailed behavior of gas molecules inside the film and clarify the mechanism of the efficient energy accommodation, the molecular beam experiments were also conducted for the free-standing films,[46] which enabled us to evaluate the interaction between VA-SWNT films and gas molecules in detail without the presence of substrates (Figure 4). In addition to the scattered molecules toward the same side as the beam incidence, the transmitted molecules through the films were also measured with the QMS positioned at the back side of the film. Since only the small fraction of the incident molecules are transmitted through the film, the molecular beam was modulated according to a maximum length sequence in order to improve the sensitivity.[47] The free-standing samples were prepared following the procedure described in Ref. 46. The VA-SWNT films were lifted off by submerging the substrates in deionized water at ~60 °C and then

re-attached on the stainless steel sample holders with a hole (2 or 4 mm in diameter). After SEM observation, selected samples with negligible amount of defects (disorder of alignment, pinholes, etc.) were used for subsequent experiments.

The scattering distribution of the transmitted molecules through the film consists of a sharply peaked component at the beam axis and a diffusive component as schematically illustrated in Figure 4. These components originate from two distinct transmission processes of gas molecules through the film, i.e. direct and diffusive transmission processes. Because of the difference in gas-surface interaction between these processes, the TOF distribution of the transmitted molecules depends on the deflection angle θ_t (Figure 5a). The TOF distribution of directly-transmitted molecules, which are distributed along the beam axis ($\theta_t = 0°$), is identical to that of the incident beam, and the distribution is independent of the surface temperature. These clearly illustrate that the molecules do not interact with SWNTs at all and preserve their incident velocities. In contrast, diffusively transmitted molecules, namely molecules transmitted off the beam axis ($\theta_t > 0°$), exhibit broader TOF distributions than the incident beam. While the transmitted molecules near the beam axis are poorly accommodated, the accommodation becomes much better as the deflection angle slightly increases. For large deflection angle, the translational energy of the transmitted molecules approaches that of the fully accommodated molecules. The reflected molecules, on the other hand, exhibit the diffusive scattering distribution independently of the incident angle. The TOF distributions (Figure 5b) show that the degree of the energy accommodation is also independent of the reflection angle θ_r, as is the case for the scattering on the as-grown VA-SWNT films on the quartz substrates with small incident angles.

The measurements with the free-standing films revealed that the scattered molecules consist of three components: reflected, diffusively transmitted, and directly transmitted molecules as shown in Figure 4. The relative amounts of each component with the incident angle of $\theta_i = 0°$ were estimated assuming that the scattering distribution is axisymmetric around the beam axis (Table 2). Most of the incident molecules are reflected even on the film with a thickness of only 0.1 μm because the frontal projected area of the randomly oriented layer is quite large in spite of the high porosity. The reflectivity of the 4-μm-thick film is similar to that of the 0.1-μm-thick film suggesting that the aligned layer of the film has a moderate influence on the gas transmissivity. The increase of the film thickness, however, leads to the more diffusive scattering distribution of the transmitted molecules (i.e. the decrease of the directly transmitted molecules) because of the increased number of collisions between gas molecules and SWNT bundles in the aligned layer. The existence of the directly-transmitted molecules is undesirable for the efficient application of VA-SWNT films as surface modification material because gas molecules reaching the substrate without the interaction with SWNTs do not contribute to the enhanced energy transfer. The amount of this component, however, is very limited even for the 0.1-μm-thick film, so that the directly-transmitted molecules do not have noticeable impact on the overall energy accommodation.

We are currently conducting a Monte Carlo simulation of molecular trajectories in VA-SWNT films in order to elucidate the mechanism of efficient energy accommodation. In this simulation, the 0.1-μm-thick free-standing film is modeled by piling up cylinders representing SWNT bundles. The preliminary result shows that incident molecules collide with SWNT bundles approximately four times on average before reflected from the film. Such multiple scattering process yields the energy accommodation coefficient roughly consistent with the

experimental result, assuming the accommodation coefficient for each collision estimated from MD simulation[31] ($\alpha \sim 0.25$). A more detailed discussion will be presented in a subsequent paper.

4. CONCLUSIONS

In summary, the scattering of helium molecules on VA-SWNT films was investigated by the molecular beam technique. We found that the modification of surfaces with VA-SWNT films significantly enhances the energy accommodation of gas molecules. The measurements with free-standing VA-SWNT films further revealed that the anomalously high energy transfer is attributed to the unique morphology of the films, where the incident gas molecules have sufficient number of collisions with SWNTs to be well accommodated. Our experiment showed that only a 100 nm thick film of VA-SWNTs significantly improves the energy accommodation of gas molecules. The films of this thickness range are readily applied to flow channels with a characteristic dimension of several μm to sub-μm, where the overall heat transfer is much influenced by the thermal conductance at gas-solid interface. Since VA-SWNT films can be prepared on surfaces directly by the CVD method or by the re-attachment technique, the surface modification with VA-SWNT films would be a promising tool for the thermal management in nano/micro devices.

AUTHOR INFORMATION

Corresponding Author

*Tel: +81-3-5841-6287. Fax: +81-3-5841-8542. E-mail: kine@fel.t.u-tokyo.ac.jp.

ACKNOWLEDGMENTS

This work was partially supported by Grant-in-Aid for Young Scientists (B) from Japan Society for the Promotion of Science (No. 23760146).

REFERENCES

(1) Yu, C.; Shi, L.; Yao, Z.; Li, D.; Majumdar, A. Thermal Conductance and Thermopower of an Individual Single-Wall Carbon Nanotube *Nano Lett.* **2005**, 5, 1842-1846.

(2) Pop, E.; Mann, D.; Wang, Q.; Goodson, K.; Dai, H. Thermal Conductance of an Individual Single-Wall Carbon Nanotube above Room Temperature *Nano Lett.* **2006**, 6, 96-100.

(3) Shiomi, J.; Maruyama, S. Molecular Dynamics of Diffusive-Ballistic Heat Conduction in Single-Walled Carbon Nanotubes *Jpn. J. Appl. Phys.* **2008**, 47, 2005-2009.

(4) Murakami, Y.; Chiashi, S.; Miyauchi, Y.; Hu, M.; Ogura, M.; Okubo, T.; Maruyama, S. Growth of Vertically Aligned Single-Walled Carbon Nanotube Films on Quartz Substrates and Their Optical Anisotropy *Chem. Phys. Lett.* **2004**, 385, 298-303.

(5) Hata, K.; Futaba, D. N.; Mizuno, K.; Namai, T.; Yumura, M.; Iijima, S. Water-Assisted Highly Efficient Synthesis of Impurity-Free Single-Walled Carbon Nanotubes *Science* **2004**, 306, 1362-1364.

(6) Zhang, G.; Mann, D.; Zhang, L.; Javey, A.; Li, Y.; Yenilmez, E.; Wang, Q.; McVittie, J. P.; Nishi, Y.; Gibbons, J. et al. Ultra-High-Yield Growth of Vertical Single-Walled Carbon

Nanotubes: Hidden Roles of Hydrogen and Oxygen *Proc. Natl. Acad. Sci. USA* **2005**, 102, 16141-16145.

(7) Zhong, G.; Iwasaki, T.; Honda, K.; Furukawa, Y.; Ohdomari, I.; Kawarada, H. Low Temperature Synthesis of Extremely Dense and Vertically Aligned Single-Walled Carbon Nanotubes *Jpn. J. Appl. Phys.* **2005**, 44, 1558-1561.

(8) Badaire, S.; Pichot, V.; Zakri, C.; Poulin, P.; Launois, P.; Vavro, J.; Guthy, C.; Chen, M.; Fischer, J. E. Correlation of Properties with Preferred Orientation in Coagulated and Stretch-Aligned Single-Wall Carbon Nanotubes *J. Appl. Phys.* **2004**, 96, 7509-7513.

(9) Zhan, G.-D.; Mukherjee, A. K. Carbon Nanotube Reinforced Alumina-Based Ceramics with Novel Mechanical, Electrical, and Thermal Properties *Int. J. Appl. Ceram. Technol.* **2004**, 1, 161-171.

(10) Haggenmueller, R.; Guthy, C.; Lukes, J. R.; Fischer, J. E.; Winey, K. I. Single Wall Carbon Nanotube/Polyethylene Nanocomposites: Thermal and Electrical Conductivity *Macromolecules* **2007**, 40, 2417-2421.

(11) Duong, H. M.; Yamamoto, N.; Bui, K.; Papavassiliou, D. V.; Maruyama, S.; Wardle, B. L. Morphology Effects on Nonisotropic Thermal Conduction of Aligned Single-Walled and Multi-Walled Carbon Nanotubes in Polymer Nanocomposites *J. Phys. Chem. C* **2010**, 114, 8851-8860.

(12) Kordás, K.; Tóth, G.; Moilanen, P.; Kumpumäki, M.; Vähäkangas, J.; Uusimäki, A.; Vajtai, R.; Ajayan, P. M. Chip Cooling with Integrated Carbon Nanotube Microfin Architectures *Appl. Phys. Lett.* **2007**, 90, 123105.

(13) Hu, M.; Shenogin, S.; Keblinski, P.; Raravikar, N. Thermal Energy Exchange Between Carbon Nanotube and Air *Appl. Phys. Lett.* **2007**, 90, 231905.

(14) Hu, M.; Shenogin, S.; Keblinski, P.; Raravikar, N. Air Flow Through Carbon Nanotube Arrays *Appl. Phys. Lett.* **2007**, 91, 131905.

(15) Yang, Z.-P.; Ci, L.; Bur, J. A.; Lin, S.-Y.; Ajayan, P. M. Experimental Observation of an Extremely Dark Material Made By a Low-Density Nanotube Array *Nano Lett.* **2008**, 8, 446-451.

(16) Tullius, J. F.; Vajtai, R.; Bayazitoglu, Y. A Review of Cooling in Microchannels *Heat Transfer Eng.* **2011**, 32, 527-541.

(17) Lu, J. W.; Day, B. S.; Fiegland, L. R.; Davis, E. D.; Alexander, W. A.; Troya, D.; Morris, J. R. Interfacial Energy Exchange and Reaction Dynamics in Collisions of Gases on Model Organic Surfaces *Prog. Surf. Sci.* **2012**, 87, 221-252.

(18) Alexander, W. A.; Zhang, J.; Murray, V. J.; Nathanson, G. M.; Minton, T. K. Kinematics and Dynamics of Atomic-Beam Scattering on Liquid and Self-Assembled Monolayer Surfaces *Faraday Discuss.* **2012**, 157, 355-374.

(19) Cohen, S. R.; Naaman, R.; Sagiv, J. Translational Energy Transfer from Molecules and Atoms to Adsorbed Organic Monolayers of Long-Chain Amphiphiles *Phys. Rev. Lett.* **1987**, 58, 1208-1211.

(20) Alexander, W. A.; Day, B. S.; Moore H. J.; Lee, T. R.; Morris, J. R.; Troya, D. Experimental and Theoretical Studies of the Effect of Mass on the Dynamics of Gas/Organic-Surface Energy Transfer *J. Chem. Phys.* **2008**, 128, 014713.

(21) Lu, J. W.; Alexander, W. A.; Morris, J. R. Gas-Surface Energy Exchange and Thermal Accommodation of CO_2 and Ar in Collisions with Methyl, Hydroxyl, and Perfluorinated Self-Assembled Monolayers *Phys. Chem. Chem. Phys.* **2010**, 12, 12533-12543.

(22) Liang, Z.; Evans, W.; Desai, T.; Keblinski, P. Improvement of Heat Transfer Efficiency at Solid-Gas Interfaces by Self-Assembled Monolayers *Appl. Phys. Lett.* **2013**, 102, 061907.

(23) Bennett, M. E.; Alexander, W. A.; Lu, J. W.; Troya, D.; Morris, J. R. Collisions of Polar and Nonpolar Gases with Hydrogen Bonding and Hydrocarbon Self-Assembled Monolayers *J. Phys. Chem. C* **2008**, 112, 17272-17280.

(24) Lu, J. W.; Morris, J. R. Gas-Surface Scattering Dynamics of CO_2, NO_2, and O_3 in Collisions with Model Organic Surfaces *J. Phys. Chem. A* **2011**, 115, 6194-6201.

(25) Alexander, W. A.; Troya, D. Theoretical Study of the Dynamics of Collisions Between HCl and ω-Hydroxylated Alkanethiol Self-Assembled Monolayers *J. Phys. Chem. C* **2011**, 115, 2273-2283.

(26) Day, B. S.; Shuler, S. F.; Ducre, A.; Morris, J. R. The Dynamics of Gas-Surface Energy Exchange in Collisions of Ar Atoms with ω-Functionalized Self-Assembled Monolayers *J. Chem. Phys.* **2003**, 119, 8084-8096.

(27) Isa, N.; Gibson, K. D.; Yan, T.; Hase, W.; Sibener, S. J. Experimental and Simulation Study of Neon Collision Dynamics with a 1-decanethiol Monolayer *J. Chem. Phys.* **2004**, 120, 2417-2433.

(28) Vázquez, S. A.; Morris, J. R.; Rahaman, A.; Mazyar, O. A.; Vayner, G.; Addepalli, S. V.; Hase, W. L.; Martínez-Núñez, E. Inelastic Scattering Dynamics of Ar from a Perfluorinated Self-Assembled Monolayer Surface *J. Phys. Chem. A* **2007**, 111, 12785-12794.

(29) Carlborg, C. F.; Shiomi, J.; Maruyama, S. Thermal Boundary Resistance Between Single-Walled Carbon Nanotubes and Surrounding Matrices *Phys. Rev. B* **2008**, 78, 205406.

(30) Bolton, K.; Gustavsson, S. Energy Transfer Mechanisms in Gas-Carbon Nanotube Collisions *Chem. Phys.* **2003**, 291, 161-170.

(31) Bolton, K.; Rosén, A. Computational Studies of Gas-Carbon Nanotube Collision Dynamics *Phys. Chem. Chem. Phys.* **2002**, 4, 4481-4488.

(32) Schiffres, S. N.; Kim, K. H.; Hu, L.; McGaughey, A. J. H.; Islam, M. F.; Malen, J. A. Gas Diffusion, Energy Transport, and Thermal Accommodation in Single-Walled Carbon Nanotube Aerogels *Adv. Funct. Mater.* **2012**, 22, 5251-5258.

(33) Scoles, G. *Atomic and Molecular Beam Methods Volume I*; Oxford University Press: New York, 1988.

(34) Harris, J. Mechanical Energy Transfer in Particle-Surface Collisions. In *Dynamics of Gas-Surface Interactions*; Rettner, C. T., Ashfold, M. N. R., Eds.; The Royal Society of Chemistry: Cambridge, 1991; pp 1-46.

(35) Einarsson, E.; Shiozawa, H.; Kramberger, C.; Rümmeli, M. H.; Grüneis, A.; Pichler, T.; Maruyama, S. Revealing the Small-Bundle Internal Structure of Vertically Aligned Single-Walled Carbon Nanotube Films *J. Phys. Chem. C* **2007**, 111, 17861-17864.

(36) Xiang, R.; Yang, Z.; Zhang, Q.; Luo, G.; Qian, W.; Wei, F.; Kadowaki, M.; Einarsson, E.; Maruyama, S. Growth Deceleration of Vertically Aligned Carbon Nanotube Arrays: Catalyst Deactivation or Feedstock Diffusion Controlled? *J. Phys. Chem. C* **2008**, 112, 4892-4896.

(37) Hu, M.; Murakami, Y.; Ogura, M.; Maruyama, S.; Okubo, T. Morphology and Chemical State of Co–Mo Catalysts for Growth of Single-Walled Carbon Nanotubes Vertically Aligned on Quartz Substrates *J. Catal.* **2004**, 225, 230-239.

(38) Kinefuchi, I.; Yamaguchi, H.; Shiozaki, S.; Sakiyama, Y.; Matsumoto, Y. Out-of-plane Scattering Distribution of Nitrogen Molecular Beam on Graphite (0001) Surface. In *RAREFIED GAS DYNAMICS: 24th International Symposium on Rarefied Gas Dynamics*; Capitelli, M., Ed.; American Institute of Physics: New York, 2005; pp 947-952.

(39) Hurst, J. E.; Becker, C. A.; Cowin, J. P.; Janda, K. C.; Wharton, L.; Auerbach, D. J. Observation of Direct Inelastic Scattering in the Presence of Trapping-Desorption Scattering: Xe on Pt(111) *Phys. Rev. Lett.* **1979**, 43, 1175-1177.

(40) Trott, W. M.; Rader, D. J.; Torczynski, J. R.; Castañeda, J. N.; Gallis, M. A.; Gochberg, L. A. Measurements of Thermal Accommodation Coefficients. In *Rarefied Gas Dynamics: 25th International Symposium on Rarefied Gas Dynamics*; Ivanov, M. S., Rebrov, A. K., Eds.; Publishing House of the Siberian Branch of the Russian Academy of Sciences: Saint Petersburg, Russia, 2007; pp 672-677.

(41) Amdur, I.; Guildner, L. A. Thermal Accommodation Coefficients on Gas-covered Tungsten, Nickel and Platinum *J. Am. Chem. Soc.* **1957**, 79, 311-315.

(42) Goodman, F. O.; Wachman, H. Y. *Dynamics of Gas-Surface Scattering*; Academic Press: New York, 1971; pp. 23-31.

(43) Hsu, I.-K.; Pettes, M. T.; Aykol, M.; Shi, L.; Cronin, S. B. The Effect of Gas Environment on Electrical Heating in Suspended Carbon Nanotubes *J. Appl. Phys.* **2010**, 108, 084307.

(44) Pettes, M. T.; Shi, L. Thermal and Structural Characterizations of Individual Single-, Double-, and Multi-Walled Carbon Nanotubes *Adv. Funct. Mater.* **2009**, 19, 3918-3925.

(45) Son, Y.; Pal, S. K.; Borca-Tasciuc, T.; Ajayan, P. M.; Siegel, R. W. Thermal Resistance of the Native Interface Between Vertically Aligned Multiwalled Carbon Nanotube Arrays and Their SiO2/Si Substrate *J. Appl. Phys.* **2008**, 103, 024911.

(46) Murakami, Y.; Maruyama, S. Detachment of Vertically Aligned Single-Walled Carbon Nanotube Films from Substrates and Their Re-attachment to Arbitrary Surfaces *Chem. Phys. Lett.* **2006**, 422, 575-580.

(47) Hirschy, V. L.; Aldridge, J. P. A Cross Correlation Chopper for Molecular Beam Modulation *Rev. Sci. Instrum.* **1971**, 42, 381-383.

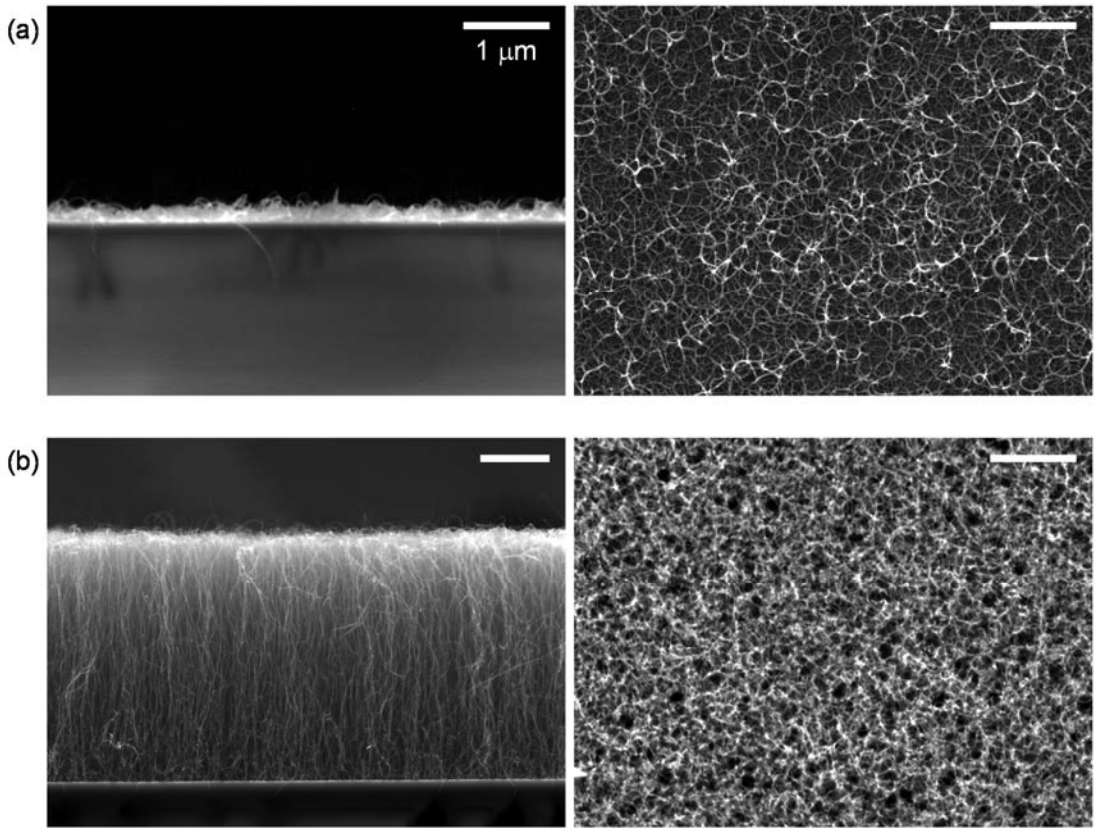

Figure 1. The SEM images of VA-SWNT films grown on quartz substrates: the side view (left) and the top view (right) of the films with thicknesses of (a) 0.1 μm and (b) 4 μm. Scale bars denotes 1 μm.

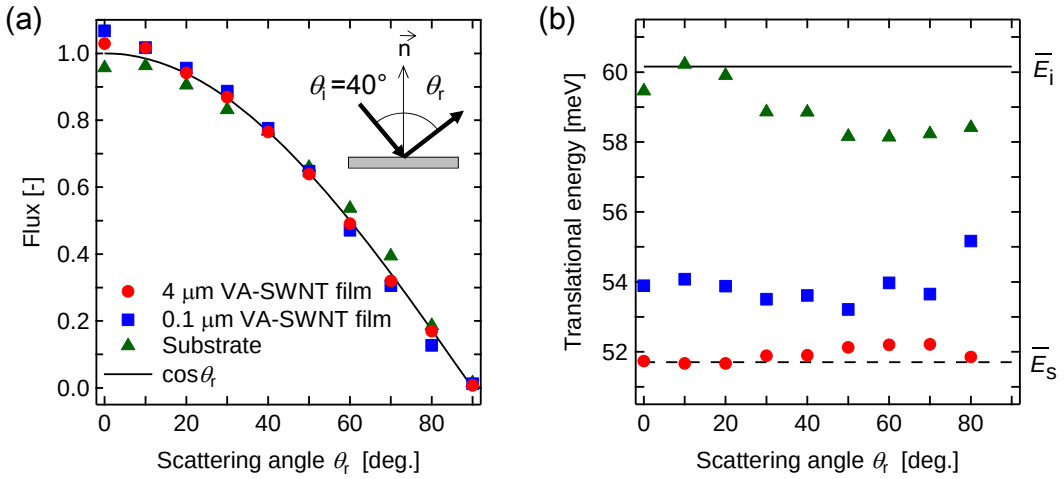

Figure 2. The scattering of helium molecules with the incident angle θ_i of 40° on a quartz substrate (▲) and VA-SWNT films with thicknesses of 0.1 μm (■) and 4 μm (●) at room temperature ($T_s \approx 300$ K). (a) The angular distributions of scattered molecules. The solid line represents the cosine distribution $\cos\theta_r$. (b) The mean translational energies of scattered molecules as a function of scattering angle. The solid and dashed lines correspond to the incident beam energy $\overline{E}_i$ = 60 meV and the mean translational energy of fully accommodated molecules $\overline{E}_s$.

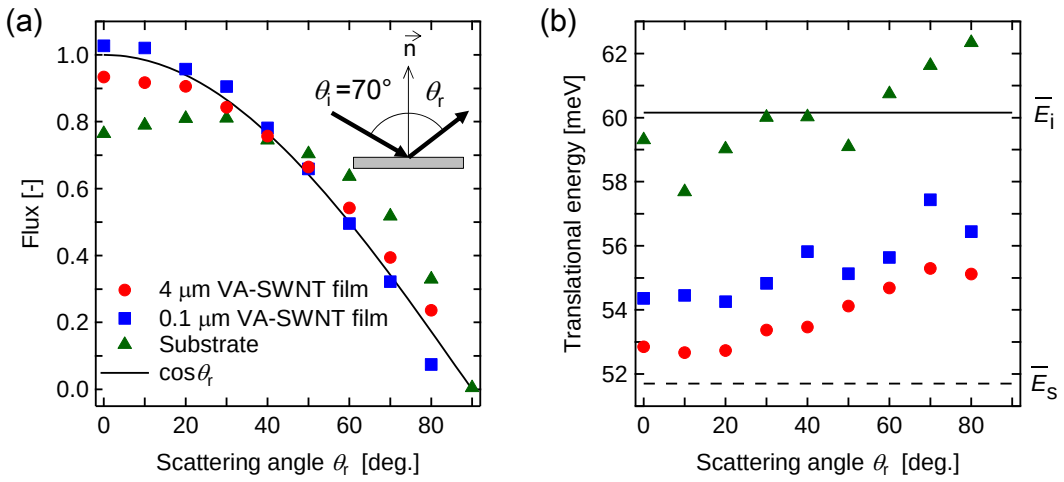

Figure 3. The scattering of helium molecules with the incident angle θ_i of 70° on a quartz substrate and VA-SWNT films with thicknesses of 0.1 μm and 4 μm at room temperature. The symbols and lines are the same as in Figure 2. (a) The angular distributions of scattered molecules. (b) The mean translational energies of scattered molecules as a function of scattering angle.

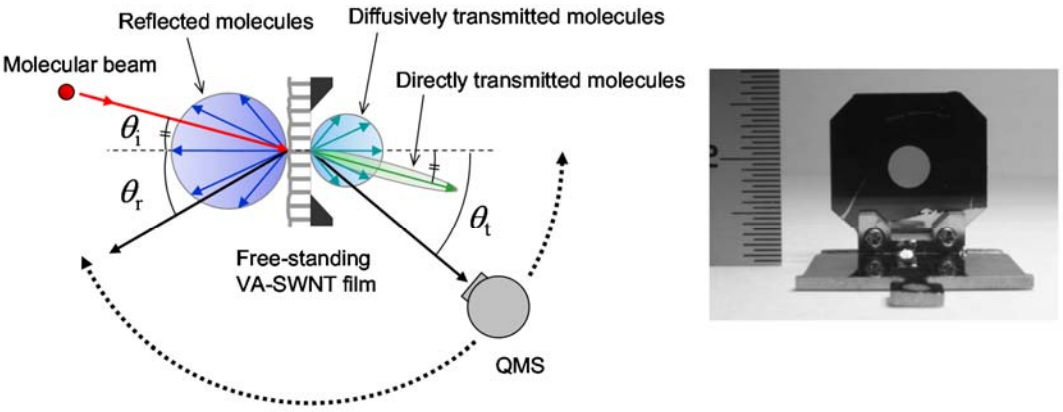

Figure 4. The schematic illustration of the measurements with free-standing VA-SWNT films. The scattering angles of reflected molecules θ_r and transmitted molecules θ_t are measured from the normal vector of the sample surface. The free-standing films were held on a stainless steel plate with a 2 or 4 mm diameter hole.

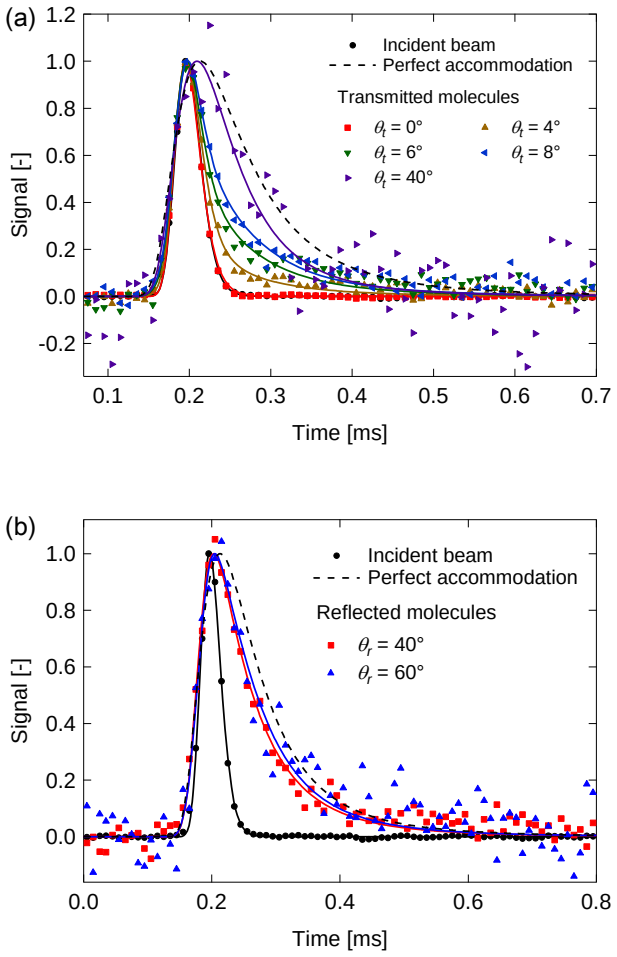

Figure 5. The TOF distributions of (a) transmitted and (b) reflected molecules from the free-standing VA-SWNT film with a thickness of 0.1 μm at room temperature. The incident angle of the helium beam was $\theta_i = 0°$. The TOF distribution of the incident beam with the film retracted from the beam path is also shown for reference. The dashed curve represents the TOF distribution calculated assuming the perfect accommodation. The definitions of the scattering angles of transmitted and reflected molecules, θ_t and θ_r, are shown in Figure 4.

Table 1. The energy accommodation coefficients of helium on surfaces at around room temperature.

Surface	α
Quartz substrate with Co-Mo nanoparticles ($\theta_i = 40°$)	0.17
4-μm-thick VA-SWNT film ($\theta_i = 40°$)	0.97
0.1-μm-thick VA-SWNT film ($\theta_i = 40°$)	0.76
304 stainless steel (machined) [40]	0.36
304 stainless steel (polished) [40]	0.40
Nickel (gas covered) [41]	0.39
Tungsten (gas covered) [41]	0.47
Platinum (gas covered) [41]	0.37

Table 2. The relative amount of each scattering component from free-standing VA-SWNT films for helium molecular beam with the incident angle of $\theta_i = 0°$.

Film thickness [μm]	Reflected molecules	Directly transmitted molecules	Diffusively transmitted molecules
0.1	0.7	0.1	0.2
4	0.7	0.005	0.3
20	1	~0	~0

TOC Graphic

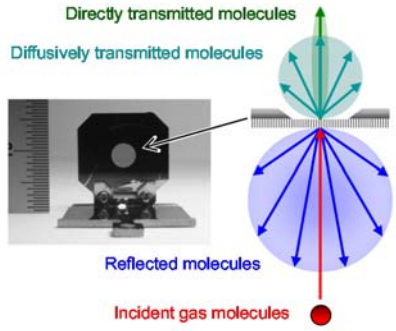
Directly transmitted molecules
Diffusively transmitted molecules
Reflected molecules
Incident gas molecules